SCIENTIFIC REP**O**RTS

OPEN

Superb electromagnetic wave-absorbing composites based on large-scale graphene and carbon nanotube films

Jinsong Li[1,2], Weibang Lu[3], Jonghwan Suhr[4], Hang Chen[5], John Q. Xiao[5] & Tsu-Wei Chou[2]

Graphene has sparked extensive research interest for its excellent physical properties and its unique potential for application in absorption of electromagnetic waves. However, the processing of stable large-scale graphene and magnetic particles on a micrometer-thick conductive support is a formidable challenge for achieving high reflection loss and impedance matching between the absorber and free space. Herein, a novel and simple approach for the processing of a CNT film-Fe_3O_4-large scale graphene composite is studied. The Fe_3O_4 particles with size in the range of 20–200 nm are uniformly aligned along the axial direction of the CNTs. The composite exhibits exceptionally high wave absorption capacity even at a very low thickness. Minimum reflection loss of -44.7 dB and absorbing bandwidth of 4.7 GHz at -10 dB are achieved in composites with one-layer graphene in six-layer CNT film-Fe_3O_4 prepared from 0.04 M $FeCl_3$. Microstructural and theoretical studies of the wave-absorbing mechanism reveal a unique Debye dipolar relaxation with an Eddy current effect in the absorbing bandwidth.

The rapid development of modern electronic equipment and wireless devices has resulted in severe electromagnetic (EM) radiation pollution, which has implications in human health and the normal functioning of electronics. Thus, the design and exploration of effective EM wave absorption materials is of basic scientific importance[1–3]. EM waves consist of a time-varying electric and magnetic field, and EM wave absorption is achieved by the attenuation of EM wave energy through dielectric loss and magnetic loss as well as electromagnetic impedance match, which can minimize the reflection of the incident EM wave[4]. Therefore, dielectric loss and magnetic loss are the main factors determining absorption capability. The dielectric tangent loss ($\tan \delta_\varepsilon = \varepsilon''/\varepsilon'$) is proportional to the dielectric loss, and it describes the dissipation of energy supplied by an external electric field as motion and heat[5]. Magnetic tangent loss ($\tan \delta_\mu = \mu''/\mu'$) is known as magnetic loss factor or power factor; it is a measure of the energy loss inside a magnetic material due to the phase delay between the applied and induced magnetic fields.

Good impedance matching between the specimen and free space is necessary for enhancing EM wave absorption capability. The impedance matching coefficient $|ZinZ0\text{-}1|$ can be expressed as[6]

$$|Z_{\mathrm{in}}/Z_0| = (\mu_r/\varepsilon_r)^{1/2} \tanh\left[j(2\pi fd/c)(\mu_r\varepsilon_r)^{1/2}\right] \tag{1}$$

And the reflection loss (RL) value is calculated according to the transmission line theory by Equation (2):

$$\mathrm{RL(dB)} = 20 \log\left|(Z_{\mathrm{in}} - Z_0)/(Z_{\mathrm{in}} + Z_0)\right| \tag{2}$$

Here, Z in is the input impedance of the absorber, Z_0 is the characteristic impedance of free space (377 Ω)[7]. $\varepsilon_r = \varepsilon' - j\varepsilon''$ and $\mu_r = \mu' - j\mu''$ are, respectively, the complex permittivity and permeability of the absorber, c is the velocity of the EM wave in free space, f is the frequency of the EM wave, and d denotes the absorber thickness.

[1]School of Physics and Nuclear Energy Engineering, Beihang University, Beijing, 100191, China. [2]Department of Mechanical Engineering, University of Delaware, Newark, DE, 19716, United States. [3]Suzhou Institute of Nano-Tech and Nano-Bionics, Chinese Academy of Sciences, Suzhou, 215123, China. [4]Department of Polymer Science and Engineering, Sungkyunkwan University, Suwon, 440-746, Republic of Korea. [5]Department of Physics and Astronomy, University of Delaware, Newark, DE, 19716, United States. Correspondence and requests for materials should be addressed to T.-W.C. (email: chou@udel.edu)

Carbon nanotubes (CNTs) offer the unique potential to be excellent EM wave absorbents. Besides their superior mechanical and thermal properties[8], the carrier mobility and current carrying capacity of CNTs is up to $10^5\,cm^2\,V^{-1}\,s^{-1}$ and $10^9\,A\,cm^{-1}$, respectively[9]. Most of the research effort to date has focused on CNTs decorated with magnetic metal or metal oxide particles for enhancing magnetic attenuation. However, the anticipated improvement in EM wave absorption performance has often been hindered by the poor dispersion of CNTs and their impedance mismatch with free space[10]. CNT films, on the other hand, not only retain the high permittivity of individual CNTs in an isotropic network structure but also greatly facilitate the dispersion of CNTs in the matrix[11]. Furthermore, the dispersion of Fe_3O_4 nanoparticles on the surface of CNTs can effectively improve permeability and impedance matching[12]. Thus, the CNT film-Fe_3O_4 absorber provides a highly desirable combination to enhance dielectric and magnetic loss and impedance matching as well as facilitate ease in composites processing.

The other focus of this research is on graphene, which is well known for its excellent electronic, chemical and physical properties[13–15]. Graphene can support current densities greater than $10^8\,A\,cm^{-2}$ [16], its carrier mobility can exceed $15,000\,cm^2\,V^{-1}\,s^{-1}$ even under ambient conditions[17], and its real and imaginary parts of the theoretical permittivity exceed 10^4 at frequency less than $400\,GHz$[18]. Theoretical studies of large-scale graphene layers have shown strong EM wave absorption for normal incident wave. The maximum absorption reaches 50 percent at six layers of graphene and one-third of the incident EM energy is dissipated at a graphene-polymer interface[19, 20]. Although large-scale multilayer graphene/methyl methacrylate for EM wave absorption has been suggested theoretically and realized in numerical simulations[18–20], large-scale graphene absorption has never been demonstrated experimentally. This is due to the fact that large-scale graphene suffers from statistical fluctuations in strength and toughness as well as impedance mismatch with free space due to the high permittivity and negligible permeability[21]. Consequently, almost all published work so far on graphene-related EM-absorbing materials has focused on graphene powder; little research has been devoted to the EM wave-absorbing performance of large-scale graphene. Moreover, in order to enhance impedance matching and absorption of both electric and magnetic fields in graphene, the improved decoration and blend of magnetic metal or metal oxide particles have become effective approaches for researchers. Some reports demonstrated that the combination of Fe_3O_4 [22–25], TiO_2 [26] and $NiFe_2O_4$ [27] magnetic nanoparticles with reduced graphene oxide powders improved the EM wave-absorbing property. However, the magnetic nanoparticles supported on graphene particles are generally aggregated, resulting in uneven distribution[25]. Therefore, the design and processing of high-performance EM-absorbing materials based on CNT and graphene remain a formidable challenge.

Here, a novel and simple approach was adopted to fabricate CNT film-Fe_3O_4 composites by the solvothermal method. The Fe_3O_4 nanoparticles on the surface of CNTs not only improved permeability but also enhanced impedance matching of the CNT film-Fe_3O_4-graphene composite. Then, the CNT film-Fe_3O_4 was used as a support substrate to prepare a large-scale graphene (LSG)-CNT film-Fe_3O_4 composite, which not only retained the dielectric performance of CNT and graphene but also avoided their aggregation.

Results

To enhance the ability of EM wave absorption, highly conductive films (thickness: $2\,\mu m$; density: $807\,mg\,cm^{-3}$) with randomly oriented CNTs coated by Fe_3O_4 nanoparticles were used as absorbing layers, the single chemical vapor deposition graphene were laid on the surface of CNT-Fe_3O_4 film as blocking layer (Supplementary Fig. S1), and the CNT film-Fe_3O_4 with epoxy resin (EPON™ Resin 862) was impedance matching layer. A schematic illustration of the fabrication process for constructing CNT film-Fe_3O_4-graphene-epoxy composites can be found as Supplementary Fig. S2.

The CNT film-Fe_3O_4 composites were processed using the solvothermal method. The morphology and diameters of the Fe_3O_4 particles prepared with different $FeCl_3$ concentrations are shown in Fig. 1. For the CNT film-Fe_3O_4 composite prepared from 0.01 M $FeCl_3$, Fe_3O_4 nanocrystals cover the CNT surface and form a few spherical particles with diameters ranging from 10–20 nm (Fig. 1a). The Fe_3O_4 particles of the as-prepared CNT film-Fe_3O_4 composite at $FeCl_3$ concentrations of 0.02–0.10 M are spherical with a uniform diameter, aligned along the axial direction of the CNTs. It should be noted that with the increase of $FeCl_3$ concentration from 0.02 to 0.10 M, the diameters of the Fe_3O_4 particles increase to a maximum value of 200 nm at 0.03 M and then decrease with a minimum value of 20–30 nm at 0.10 M (Fig. 1b–f). Such observations provide clear evidence of the direct relationship between Fe_3O_4 nanoparticle size and $FeCl_3$ concentration. The growth of the Fe_3O_4 nanoparticles follows the two-stage growth model, in which nanocrystals nucleate first and then aggregate into larger particles on the CNT surface[28].

Figure 1g is a TEM image of a CNT film-Fe_3O_4-0.04 M graphene composite. Crystal planes are identified in the selected-area electron diffraction pattern (Fig. 1h), which is consistent with the XRD pattern. Figure 2a shows the XRD patterns of the pure CNT film and CNT film-Fe_3O_4 composites prepared at various $FeCl_3$ concentrations. The peak positions and relative intensities match well with the standard XRD data (JCPDS no. 19–0629), and the seven peaks at 18.17°, 30.07°, 35.48°, 43.01°, 53.42°, 57.04° and 62.55° are associated with the (111), (220), (311), (400), (422), (511) and (440) crystal planes of Fe_3O_4, respectively. No additional peaks belonging to other phases are observed, indicating the good crystallinity and high purity of the Fe_3O_4 nanoparticles. The energy dispersive spectroscopy (EDS) as shown in Fig. 1b reveals that the CNT film-Fe_3O_4–0.05 M composite is mainly composed of C, O, and Fe elements.

The average sizes of nanocrystals in the Fe_3O_4 nanoparticles are calculated for the strongest peak (311) by the Debye–Scherrer formula. The nanocrystal sizes from the data of Fig. 2 are 9.7, 14.5, 16.4, 18.7, 22.3 and 27.2 nm for CNT film-Fe_3O_4 composites prepared from 0.01, 0.02, 0.03, 0.04, 0.05 and 0.10 M $FeCl_3$, respectively; this implies that the nanocrystal size increases significantly with increasing concentration of $FeCl_3$. The saturation magnetization and relaxation values are directly related to the size of the nanocrystal size, and with the increase of Fe_3O_4 nanocrystal size, both the saturation magnetization and relaxation rate increase[29].
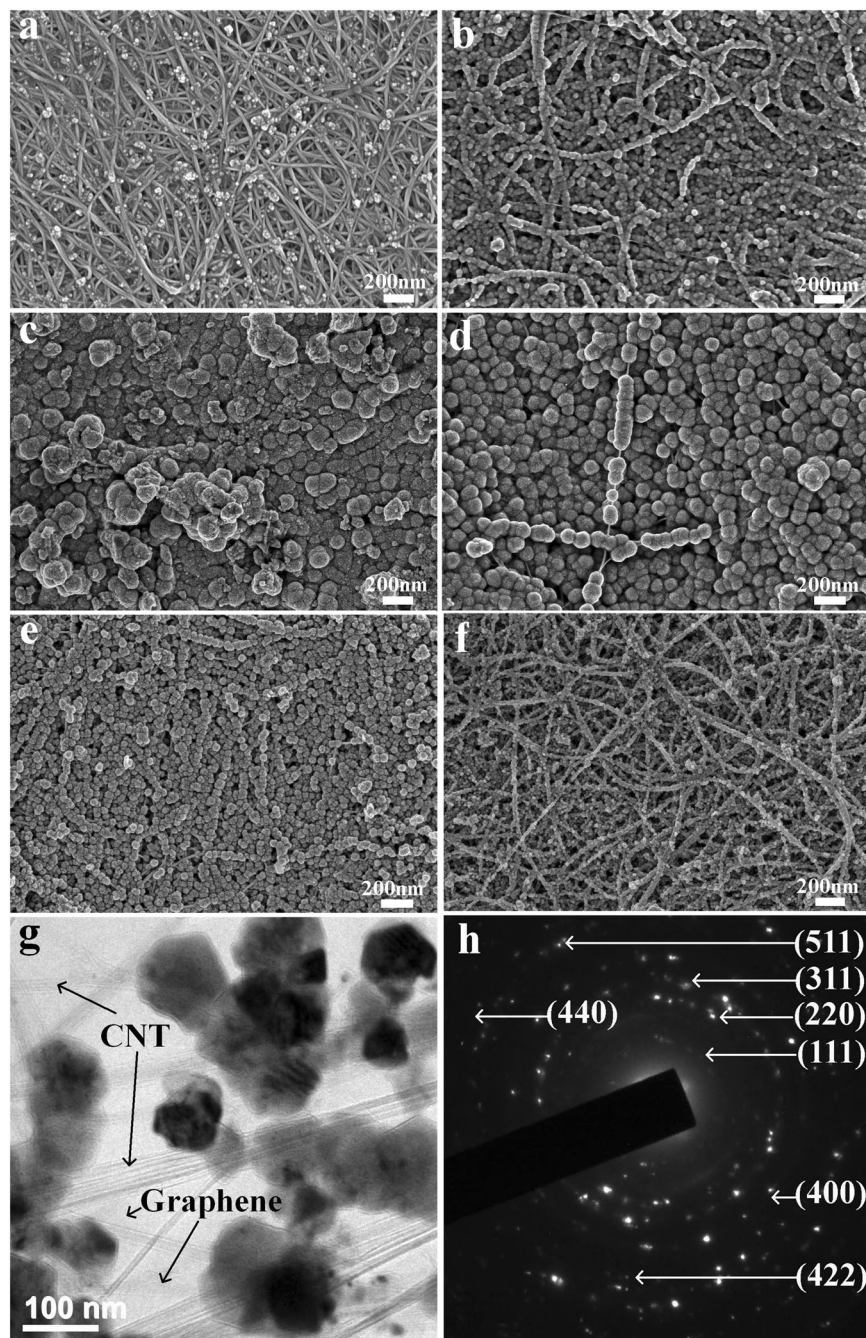
Figure 1. Scanning electron microscope images of the composite prepared at $FeCl_3$ concentrations of 0.01–0.10 M: (**a**) 0.01 M, (**b**) 0.02 M, (**c**) 0.03 M, (**d**) 0.04 M, (**e**) 0.05 M and (**f**) 0.10 M. (**g**) Transmission electron microscopy of CNT film-Fe_3O_4-0.04 M-graphene. (**h**) The selected-area electron diffraction pattern of Fe_3O_4 nanoparticle.

The magnetic properties of the CNT film-Fe_3O_4 composites at room temperature are shown in Fig. 3. Significant hysteresis loops indicate the ferromagnetic behavior of CNT film-Fe_3O_4 composites (Fig. 3a). The saturation magnetization (M_s) and remnant magnetization (M_r) of the CNT film-Fe_3O_4-0.01 M and 0.02 M remain nearly the same as those of the CNT film. At $FeCl_3$ concentrations higher than 0.02 M, the M_s and M_r values increase rapidly, as shown in Fig. 3b and c. The variation of coercivity (H_c) with $FeCl_3$ concentration is shown in Fig. 3d. The values of μ_r and anisotropy energy, which are related to the values of M_s and H_c, affect the EM wave absorption capacities[30].

Based on the above magnetic property data and morphology observations, CNT film-Fe_3O_4-0.05 M composites with various numbers of layers were fabricated. The values of $\tan \delta_\varepsilon$ and $\tan \delta_\mu$, impedance matching coefficient $|Z_{in}/Z_0|$ and reflection loss of composites consisting of one to seven CNT film-Fe_3O_4-0.05 M layers were deduced from the measured data of relative complex permittivity ε_r, permeability μ_r and thickness d. The
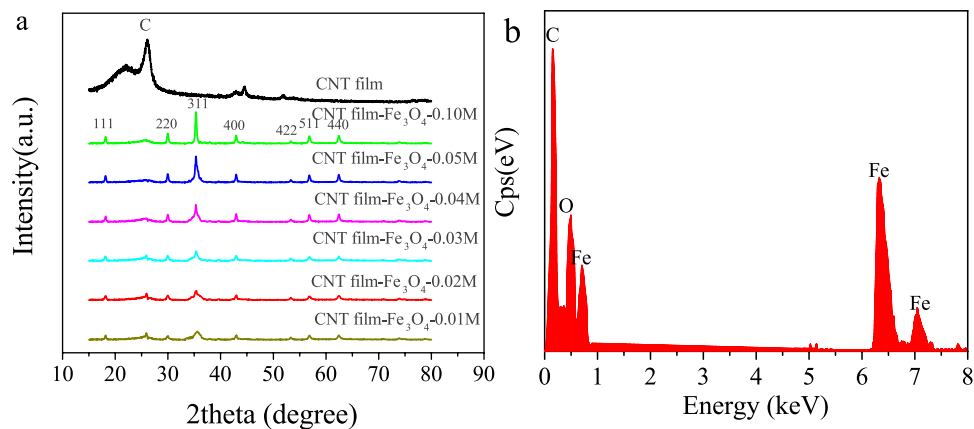
Figure 2. (**a**) XRD patterns of CNT film-Fe$_3$O$_4$ composite. (**b**) EDS pattern of CNT film-Fe$_3$O$_4$-0.05 M composite.
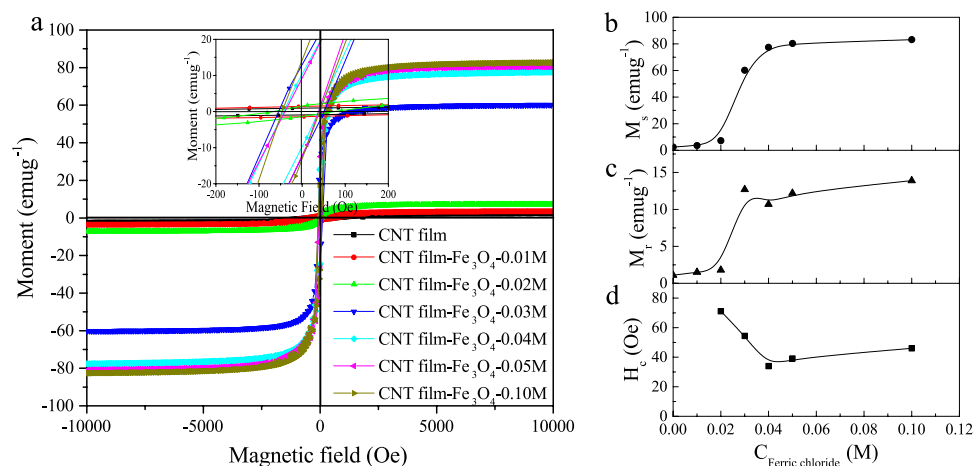
Figure 3. (**a**) Magnetic hysteresis loops of composites at room temperature (inset shows expanded low field hysteresis curves). (**b**) Variation of saturation magnetization with FeCl$_3$ concentration. (**c**) Variation of remnant magnetization with FeCl$_3$ concentration. (**d**) Variation of coercivity with FeCl$_3$ concentration.

effect of the number of layers on the composite EM wave-absorbing properties was studied. The results of Fig. 4a demonstrate that strong peaks of tan δ$_ε$ appear when the frequency is higher than 6 GHz. The locations of peaks shift toward lower frequencies with an increase in the number of layers of CNT film-Fe$_3$O$_4$ composite. The peak intensity varies with the number of layers and reaches a maximum value of 1.72 at four layers. Figure 4b depicts the variation of tan δ$_μ$ of the CNT film-Fe$_3$O$_4$ composites with frequency and number of layers. Strong peaks of tan δ$_μ$ can be seen in the frequency range of 10–17 GHz, and the peak location also shifts toward lower frequencies with increasing number of layers. The peak intensity of tan δ$_μ$ decreases from a maximum value of 0.58 at one layer to a minimum value of 0.08 at four layers. It should be noted that the values of tan δ$_μ$ become negative in some frequency ranges, indicating that the magnetic energy radiated out from the composites due to the high carrier mobility of CNTs[7]. Overall, the above results demonstrate the dependence of the dielectric and magnetic responses on the number of layers of CNT film-Fe$_3$O$_4$ composite. In addition, the values of tan δ$_ε$ are larger than those of tan δ$_ε$ for almost the entire frequency range, suggesting that dielectric loss plays a major role in the intrinsic EM wave absorption.

Results of $|Z_{in}/Z_0|$ and RL calculated from the relative permittivity and permeability data are given in Fig. 4c and d, respectively. When $|Z_{in}/Z_0|$ is close to unity, most of the EM waves can effectively enter the composite and then dissipate as heat. Figure 4c shows that when the number of layers is increased, the value of $|Z_{in}/Z_0|$ of the CNT film-Fe$_3$O$_4$ composites increases and reaches a maximum value of 1.73 at six layers and then decreases to 0.80 at seven layers. Only the values of $|Z_{in}/Z_0|$ of the CNT film-Fe$_3$O$_4$ composites with five and six layers are close to unity in the frequency range of 10–17 GHz. Figure 4d shows that for the CNT film-Fe$_3$O$_4$ composite with five layers, the minimum value of reflection loss is −19.3 dB, and the frequency bandwidth at −10 dB is 3.6 GHz. For the CNT film-Fe$_3$O$_4$ composite with six layers, the minimum value of reflection loss is −26.6 dB, and the frequency bandwidth at −10 dB is 2.9 GHz. However, although the CNT film-Fe$_3$O$_4$ composites with one, two,
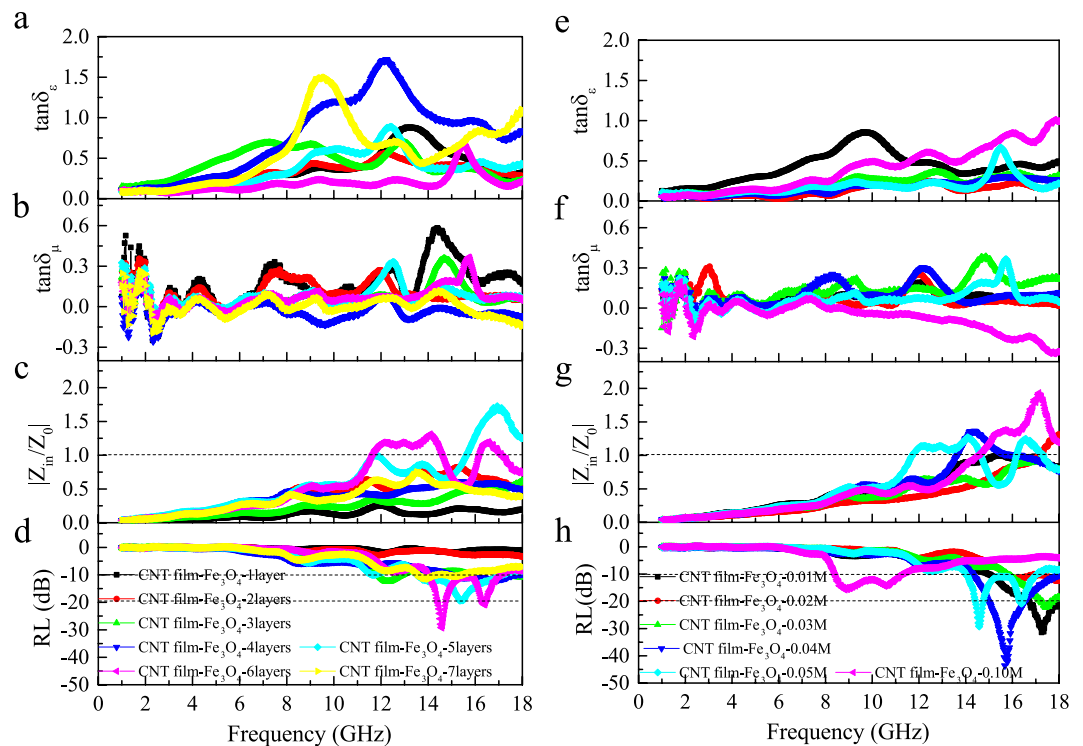
Figure 4. (**a**) Dielectric tangent loss, (**b**) magnetic tangent loss, (**c**) impedance matching coefficient $|Z_{in}/Z_0|$ and (**d**) reflection loss of the CNT film-Fe_3O_4 composites with one, two, three, four, five, six and seven layers prepared from 0.05 M $FeCl_3$. (**e**) Dielectric tangent loss, (**f**) magnetic tangent loss, (**g**) impedance matching coefficient $|Z_{in}/Z_0|$ and (**h**) reflection loss of the CNT film-Fe_3O_4 composites with six layers prepared from 0.01, 0.02, 0.03, 0.04, 0.05 and 0.10 M $FeCl_3$.

three, four and seven layers have higher dielectric loss, the frequency bandwidth at −10 dB and the magnitude of minimum reflection loss are far less than those of five- and six-layer composites.

Based on the results of CNT film-Fe_3O_4 composites with different layers, CNT film-Fe_3O_4 composites of six layers with different $FeCl_3$ concentrations were prepared. As shown in Fig. 4e and f, the values of tan δ_ε of the CNT film-Fe_3O_4 composites of 0.02–0.05 M are all less than that of the CNT film-Fe_3O_4-0.01 M composite, and the values of tan δ_μ are all higher than that of the CNT film-Fe_3O_4-0.01 M composite. It is interesting that tan δ_ε of the CNT film-Fe_3O_4-0.10 M increases almost monotonically with frequency. The tan δ_μ value of the CNT film-Fe_3O_4-0.10 M is negative and shows a decreasing trend at frequencies higher than 8.5 GHz (Fig. 4f). Figure 4g shows that the $|Z_{in}/Z_0|$ values of some composites are close to unity at frequencies higher than 11.7 GHz. The minimum values of reflection loss of the CNT film-Fe_3O_4-0.01, 0.04 and 0.05 M composites are -32.0 dB at 17.1 GHz, −43.6 dB at 15.7 GHz and −26.6 dB at 14.5 GHz, respectively, obviously shifting to lower frequency range with increase in $FeCl_3$ concentrations (Fig. 4h). For the same composites, the bandwidths of the reflection loss at −10 dB are 3.1 GHz, 3.7 GHz and 2.9 GHz, respectively; their bandwidths of reflection loss at −20 dB are 1.2 GHz, 1.5 GHz and 0.3 GHz, respectively. Although the CNT film-Fe_3O_4-0.10 M composite has no strong RL peak, the bandwidth at −10 dB is 2.9 GHz.

On the basis of the results summarized above, CNT film-Fe_3O_4-LSG composites with six layers of CNT film-Fe_3O_4-0.04 M and various numbers of graphene layers have been processed and studied. Although the minimum reflection loss and thickness of the CNT film-Fe_3O_4 composite established from the above experiments are highly encouraging, the absorption bandwidth of 3.7 GHz is still relatively small. To further improve the EM wave-absorption performance, it is desirable to pursue a CNT film-Fe_3O_4-graphene composite in which the graphene layers are separated from one another by a thin layer of epoxy. Figure 5a and b show that tan δ_ε increases and tan δ_μ decreases to negative values with an increasing number of graphene layers; the ranges of tan δ_ε and tan δ_μ are, respectively, 0.2–1.6 and −0.4–0.1 for the frequencies of 3–18 GHz, indicating that the dielectric loss plays a major role in EM wave absorption.

In addition, EM wave attenuation in an absorber is a key factor for achieving EM wave absorption. The EM wave attenuation ability of an absorber can be characterized by the attenuation constant[30]

$$\alpha = \sqrt{2}\pi f c^{-1}\sqrt{(\varepsilon''\mu'' - \varepsilon'\mu') + \sqrt{(\varepsilon''\mu'' - \varepsilon'\mu')^2 + (\varepsilon'\mu'' - \varepsilon''\mu')^2}} \tag{3}$$

The results of Fig. 5c show that all samples exhibit a high attenuation constant (larger than 150) in the frequency range of 7–18 GHz. The values of α increased with an increasing number of graphene layers, and an obvious peak appears when the number of graphene layers is less than four. The locations of peaks shift toward higher frequencies as the number of graphene layers increases. Figure 5d shows the variations of impedance matching
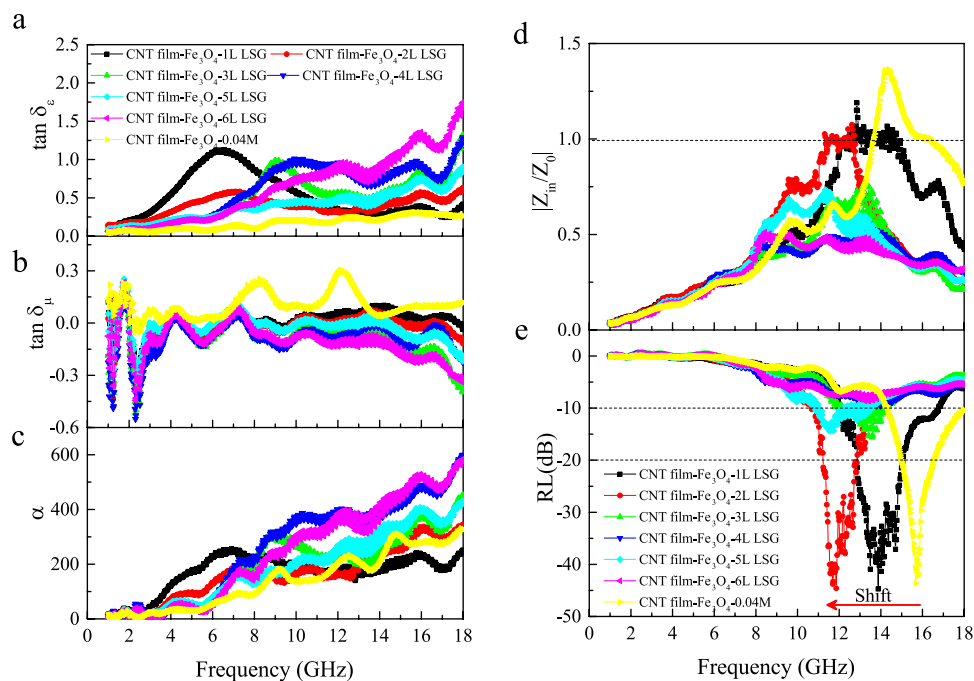
Figure 5. (**a**) Dielectric tangent loss, (**b**) magnetic tangent loss, (**c**) attenuation constant, (**d**) impedance matching coefficient $|Z_{in}/Z_0|$ and (**e**) reflection loss of the CNT film-Fe$_3$O$_4$-0.04 M-LSG composites with one, two, three, four, five and six layers of graphene.

coefficient $|Z_{in}/Z_0|$ with frequency. The $|Z_{in}/Z_0|$ values of CNT film-Fe$_3$O$_4$–1L and 2L LSG composites are close to unity in the frequencies of 11–15 GHz, and the corresponding impedance matching bandwidth of frequency is enhanced by the large-scale graphene compared to that of the CNT film-Fe$_3$O$_4$-0.04 M composite without LSG. However, the $|Z_{in}/Z_0|$ values decrease with the increase of graphene layers.

As shown in Fig. 5e, for the CNT film-Fe$_3$O$_4$-0.04 M-1L LSG composite, the reflection loss is below −10 dB at 12.0–16.7 GHz, and the minimum value is −44.7 dB at 13.9 GHz; the bandwidths of the reflection loss at −10 dB and −20 dB are 4.7 GHz and 2.2 GHz, respectively. Compared to the CNT film-Fe$_3$O$_4$-0.04 M composite without graphene, the bandwidths of the reflection loss at −10 dB and −20 dB increase by 27.0 percent and 46.7 percent, respectively; the minimum reflection loss increases by 2.5 percent, and the peak of the reflection loss shifts from 15.7 GHz to 13.9 GHz. For the case of two graphene layers, the reflection loss is below −10 dB at 10.9–13.5 GHz, and the minimum value is −44.6 dB at 11.9 GHz; the bandwidths of the reflection loss at −10 dB and −20 dB are 2.6 GHz and 1.6 GHz, respectively. However, with the further increase of graphene from three to six layers, the absorbing performance deteriorates sharply; the reflection loss has no bandwidth under −20 dB, and there is only a narrow bandwidth at −10 dB.

Discussion

An important mechanism of dielectric loss, which arises from the polarization and its associated relaxation, can be evaluated by the Cole–Cole semicircle (ε'' versus ε'), and each semicircle is correlated with one Debye relaxation process[7]. The Cole–Cole semicircles of the composite samples are shown in Fig. 6a–e. For the CNT film-Fe$_3$O$_4$-1L LSG composite, one large Cole-Cole semicircle, which consists of many tiny semicircles, and three small semicircles can be identified in Fig. 6a. With an increasing number of graphene layers, the number of Cole–Cole semicircles increases (Fig. 6b–e), the large semicircle decreases in size, and the tiny semicircles increase in size. The presence of semicircles in the $\varepsilon'' \sim \varepsilon'$ relation provides the evidence that there are dual dielectric relaxation processes in the CNT film-Fe$_3$O$_4$-LSG composites and demonstrates that large-scale graphene improves the intensity of the Debye dipolar relaxation process[31].

In the microwave frequency band, magnetic loss mainly comes from the eddy current effect, along with natural and exchange resonance[6]. The eddy current loss contribution to the imaginary part of permeability is related to the permeability of vacuum (μ_0), thickness (d) and electrical conductivity (σ) of the composite as $\mu'' = 2\pi\mu_0(\mu')^2\sigma d^2 f/3$. If the magnetic loss results from the eddy current effect, $\mu''(\mu')^{-2}f^{-1}$ should be constant when the frequency varies. It is shown in Fig. 6f that the values of $\mu''(\mu')^{-2}f^{-1}$ drastically fluctuate in the frequency range of 2.0–8.0 GHz. However, when f >8.0 GHz, the values of $\mu''(\mu')^{-2}f^{-1}$ remain essentially constant. Thus, it can be concluded that the magnetic loss at 2.0–8.0 GHz is caused by natural resonance, and the other peaks at 8.0–18.0 GHz are ascribed to the eddy current effect.

A superb EM wave-absorbing material is expected to possess not only a high RL factor and broad absorption bandwidth, but also a fine thickness and, hence, light weight. The reflection loss, absorption bandwidth and thickness achieved in the composites of this work are shown in Fig. 7 and compared with those of previously reported graphene- and CNT-based EM wave-absorbing composites. Compared to other graphene particle or CNT-based
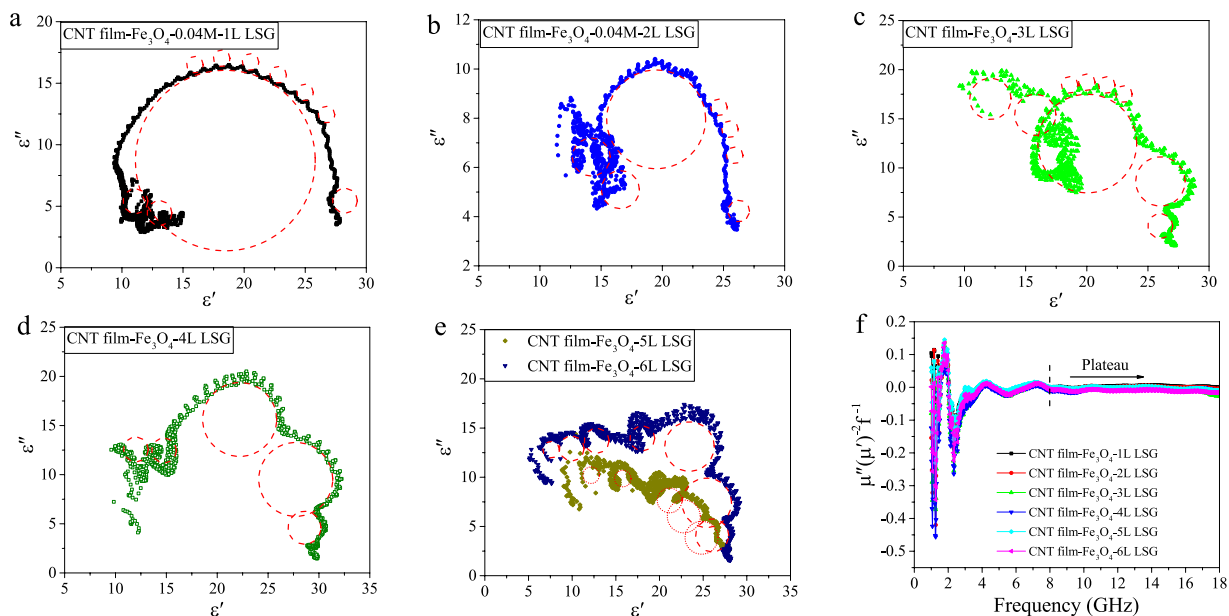
Figure 6. Dielectric Cole-Cole semicircles of the CNT film-Fe_3O_4-0.04 M-LSG composites: (**a**) one, (**b**) two, (**c**) three, (**d**) four, (**e**) five and (**f**) six layers of graphene, respectively. (**f**) $\mu''(\mu')^{-2}f^{-1}$ vs. frequency f for the CNT film-Fe_3O_4-0.04 M-LSG composites.
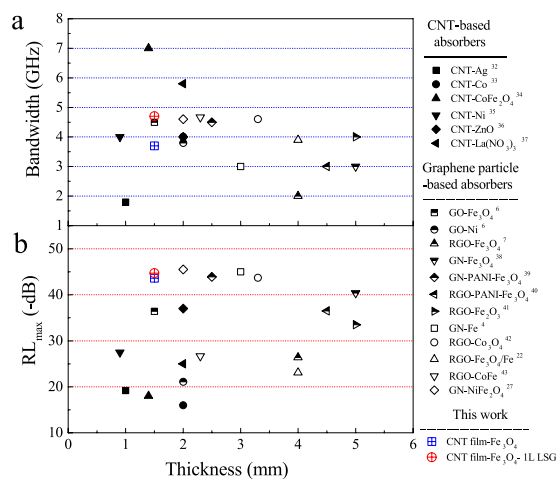
Figure 7. Maximum of reflection loss, absorbing bandwidth and thickness of this work compared with those of previously reported graphene- and CNT-based wave-absorbing composites: (**a**) absorbing bandwidth at −10 dB, (**b**) maximum of reflection loss. (GN: graphene; GO: graphene oxide; RGO: reduced graphene oxide[4, 6, 7, 22, 27, 35–46].

absorbers, the absorption bandwidth achieved in this work is 0.6–161.1 percent higher than the others except for the CNT-$CoFe_2O_4$ and CNT-$La(NO_3)_3$ absorbers (Fig. 7a); the composite thickness of this work is reduced by 25–70 percent except for the CNT-Ni, -Ag and -$La(NO_3)_3$ absorbers at 0.9, 1 and 1.4 mm, respectively, and the GO-Fe_3O_4 absorber also at 1.5 mm. However, the maximum reflection loss of this work is 1.2–2.5 times the values of the above five absorbers CNT-Ni, -Ag and -$CoFe_2O_4$ and -$La(NO_3)_3$, GO-Fe_3O_4 (Fig. 7b).

In summary, we have demonstrated that composites composed of large-scale graphene and CNT film-Fe_3O_4 substrate demonstrate superb EM wave-absorbing performance. Through optimization of the number of layers of CNT film-Fe_3O_4 composite and $FeCl_3$ concentrations, the CNT film-Fe_3O_4-LSG-epoxy composites are processed using six layers of CNT film-Fe_3O_4 prepared from 0.04 M $FeCl_3$. The CNT film-Fe_3O_4-1L LSG-epoxy composite has the highest wave-absorbing capability. Increasing the number of layers of graphene leads to an increase in wave attenuation ability but a decrease in impedance matching coefficient and a corresponding decrease in minimum reflection loss and absorbing bandwidth. Compared to the CNT film-Fe_3O_4-0.04 M composite without graphene, the minimum reflection loss and absorption bandwidth at −10 dB of the corresponding composite with one-layer graphene increase by 27.0 percent and 2.5 percent, respectively. This study provides a thorough
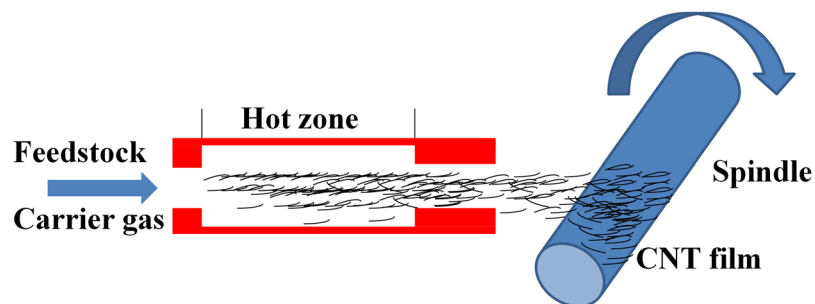
Figure 8. Schematics of CNT film fabrication.

explanation of nanocarbon-based electromagnetic wave-absorbing composites and opens up the opportunity to apply large-scale CNT and graphene films for EM wave absorption.

Methods

Sample preparation process.   CNT film was fabricated by floating catalyst chemical vapor deposition (FCCVD) method[32]. Figure 8 shows the schematics of CNT film fabrication. In this process, the feedstock of ethanol containing 1.2 vol % ferrocene and 0.4 vol % thiophene, carried by Ar/H_2, was injected at the rate of 20 mL/h into a reactor at high temperature (~1300 °C). Ethanol, ferrocene, and thiophene were used as carbon source, catalyst precursor, and promotor, respectively. CNTs were synthesized and entangled in the hot zone forming a stocking-like aerogel. The CNT aerogel was then blown out continuously from the reactor and collected layer-by-layer by a wheel rotating perpendicularly to the gas flow, which formed macroscopic CNT film (thickness: 2 μm; density: 807 mg/cm^3) with randomly oriented CNTs[33]. This CNT film was further densified by spraying ethanol onto it to enhance its mechanical and physical properties.

The single-layer graphene films were synthesized on a Cu substrate using the CVD method. A Cu foil was annealed at 1000 °C for 1.5 h in a quartz tube with a 2 sccm H_2 flow. Subsequently, a 20 sccm CH_4 flow was introduced for graphene growth at 30 mTorr for 0.5 h. Then, the furnace was quickly cooled to room temperature under He flow, and the single-layer graphene on Cu foil was obtained[34]. The size of the graphen was 25 mm × 20 mm.

The CNT film-Fe_3O_4 composites were prepared in a solvothermal system by the reduction reaction between $FeCl_3$ and ethylene glycol in the presence of CNT film. $FeCl_3 \cdot 6H_2O$ was dissolved into 50 mL ethylene glycol followed by the addition of 3.0 NaAc (protective agent) and 10 mL ethylene diamine (EDA) to form a homogeneous solution with magnetic stirring. The mixture was then transferred to a 100 mL Teflon-lined stainless steel autoclave, and 30 cm^2 CNT film was completely immersed in the solution for solvothermal reaction at 200 °C for 10 h (Supplementary Fig. S3). After washed with deionized water five times and dried under vacuum at 70 °C for 20 min, the prepared production was cut uniformly into six pieces with dimensions 25 mm × 20 mm. The loading Fe_3O_4 prepared at $FeCl_3$ concentrations of 0.01, 0.2, 0.3, 0.4, 0.5 and 0.10 M were 2, 4, 6, 6, 5 and 3×10^{-5} g/cm^2, respectively. The Cu foil of the PMMA-graphene-copper foil was etched away by 0.2 gml^{-1} $FeCl_3$. After rinsing with deionized water, the floating PMMA/graphene film was scooped up by CNT film-Fe_3O_4 film. Then, the precoated PMMA was dissolved by acetone. Finally, the laminated graphene on CNT film-Fe_3O_4 substrate was obtained.

The individual CNT-Fe_3O_4-graphene films were first sprayed with a diluted epoxy solution prepared by mixing an epoxy base agent (EPON^{TM} Resin 862), curing agent (DETDA) and ethyl acetate in the ratio of 10:1:100, followed by degassing in a vacuum oven for 30 min. Next, a CNT film-Fe_3O_4-graphene-epoxy composite was prepared by laminating the as fabricated films by spin coating Resin 862 and DETDA in the ratio of 10:1, followed by curing at 100 °C for 1 h. The thickness of one layer of CNT film-Fe_3O_4-epoxy composite was about 0.25 mm.

Characterization.   X-ray diffraction (XRD) patterns of the composites were measured on a Bruker D8 advance diffractometer using a Cu Kα source ($\lambda = 0.154056$ nm). Scanning electron microscopy (SEM) and transmission electron microscope (TEM) images were performed on the Auriga 60 and TEM Talos F200C, respectively. A magnetic study was performed by a vibrating sample magnetometer (VSM, Quantum Design, Versalab). The electromagnetic parameters of the samples were measured using a vector network analyzer (Agilent 8722ES) in the range of 1-18 GHz after a full two-port calibration (Supplementary Fig. S4–S6). The composite was machined into a toroidal shaped sample with an outer diameter of 7.0 mm and inner diameter of 3.04 mm.

Data Availability.   All data generated or analysed during this study are included in this published article (and its Supplementary Information files).

References

1. Ohkoshi, S. *et al.* A millimeter-wave absorber based on gallium-substituted epsilon-iron oxide nanomagnets. *Angew. Chem., Int. Ed.* **46**, 8392–8395 (2007).
2. Qin, F. & Brosseau, C. A review and analysis of microwave absorption in polymer composites filled with carbonaceous particles. *J. Appl. Phys.* **111**, 061301 (2012).
3. Sun, G., Dong, B., Cao, M., Wei, B. & Hu, C. Hierarchical dendrite-like magnetic materials of Fe_3O_4, γ-Fe_2O_3, and Fe with high performance of microwave absorption. *Chem. Mater.* **23**, 1587–1593 (2011).
4. Zhao, X. *et al.* Excellent microwave absorption property of graphene-coated Fe nanocomposites. *Sci. Rep.* **3**, 3421 (2013).

8

5. Salter, D. C. Energy Basis of Dielectric-Relaxation Loss. *Nature* **271**, 645–648 (1978).
6. Wang, G. *et al*. High densities of magnetic nanoparticles supported on graphene fabricated by atomic layer deposition and their use as efficient synergistic microwave absorbers. *Nano Res* **7**, 704–716 (2014).
7. Sun, X. *et al*. Laminated magnetic graphene with enhanced electromagnetic wave absorption properties. *J. Mater. Chem. C* **1**, 765–777 (2013).
8. Baughman, R. H., Zakhidov, A. A. & de Heer, W. A. Carbon nanotubes–the route toward applications. *Science* **297**, 787–792 (2002).
9. Zhou, Y. X. *et al*. p-channel, n-channel thin film transistors and p-n diodes based on single wall carbon nanotube networks. *Nano Lett.* **4**, 2031–2035 (2004).
10. Wang, L.-L. *et al*. Electromagnetic interference shielding effectiveness of carbon-based materials prepared by screen printing. *Carbon* **47**, 1905–1910 (2009).
11. Xu, H., Tong, X., Zhang, Y., Li, Q. & Lu, W. Mechanical and electrical properties of laminated composites containing continuous carbon nanotube film interleaves. *Compos. Sci. Technol.* **127**, 113–118 (2016).
12. Pawar, S. P., Marathe, D. A., Pattabhi, K. & Bose, S. Electromagnetic interference shielding through MWNT grafted Fe_3O_4 nanoparticles in PC/SAN blends. *J. Mater. Chem. A* **3**, 656–669 (2015).
13. Balandin, A. A. *et al*. Superior thermal conductivity of single-layer graphene. *Nano Lett.* **8**, 902–907 (2008).
14. Castro Neto, A. H., Guinea, F., Peres, N. M. R., Novoselov, K. S. & Geim, A. K. The electronic properties of graphene. *Rev. Mod. Phys.* **81**, 109–162 (2009).
15. Novoselov, K. S. *et al*. Electric field effect in atomically thin carbon films. *Science* **306**, 666–669 (2004).
16. Geim, A. K. & Novoselov, K. S. The rise of graphene. *Nat. Mater.* **6**, 183–191 (2007).
17. Schwierz, F. Graphene transistors. *Nat. Nanotechnol.* **5**, 487–496 (2010).
18. Li, Q. *et al*. Active graphene-silicon hybrid diode for terahertz waves. *Nat. Commun.* **6**, 7082 (2015).
19. Batrakov, K. *et al*. Flexible transparent graphene/polymer multilayers for efficient electromagnetic field absorption. *Sci. Rep.* **4**, 7191 (2014).
20. Lobet, M., Majerus, B., Henrard, L. & Lambin, P. Perfect electromagnetic absorption using graphene and epsilon-near-zero metamaterials. *Phys. Rev. B* **93**, 235424 (2016).
21. Shekhawat, A. & Ritchie, R. O. Toughness and strength of nanocrystalline graphene. *Nat. Commun.* **7**, 10546 (2016).
22. Ding, Y. *et al*. Electromagnetic wave absorption in reduced graphene oxide functionalized with Fe_3O_4/Fe nanorings. *Nano Res.* **9**, 2018–2025 (2016).
23. Yin, Y. *et al*. Enhanced high-frequency absorption of anisotropic Fe_3O_4/graphene nanocomposites. *Sci. Rep.* **6**, 25075 (2016).
24. Zhang, R. *et al*. Enhanced microwave absorption properties of ferroferric oxide/graphene composites with a controllable microstructure. *RSC Adv.* **6**, 16952–16962 (2016).
25. Zheng, X. L. *et al*. Hydrophobic graphene nanosheets decorated by monodispersed superparamagnetic Fe_3O_4 nanocrystals as synergistic electromagnetic wave absorbers. *J. Mater. Chem. C* **3**, 4452–4463 (2015).
26. Liu, P. B., Huang, Y., Yan, J. & Zhao, Y. Magnetic graphene@PANI@porous TiO_2 ternary composites for high-performance electromagnetic wave absorption. *J. Mater. Chem. C* **4**, 6362–6370 (2016).
27. Liu, P., Huang, Y. & Zhang, X. Superparamagnetic $NiFe_2O_4$ particles on poly(3,4-ethylenedioxythiophene)–graphene: Synthesis, characterization and their excellent microwave absorption properties. *Compos. Sci. Technol.* **95**, 107–113 (2014).
28. Ge, J., Hu, Y., Biasini, M., Beyermann, W. P. & Yin, Y. Superparamagnetic magnetite colloidal nanocrystal clusters. *Angew. Chem. Int. Ed.* **46**, 4342–4345 (2007).
29. Xuan, S., Wang, Y.-X. J., Yu, J. C. & Cham-Fai Leung, K. Tuning the grain size and particle size of superparamagnetic Fe_3O_4 microparticles. *Chem. Mater.* **21**, 5079–5087 (2009).
30. Lu, B. *et al*. Influence of alloy components on electromagnetic characteristics of core/shell-type Fe–Ni nanoparticles. *J. Appl. Phys.* **104**, 114313 (2008).
31. Bagchi, B. & Chandra, A. Dielectric relaxation in dipolar liquids: Route to Debye behavior via translational diffusion. *Phys. Rev. Lett.* **64**, 455–458 (1990).
32. Xu, H., Tong, X., Zhang, Y., Li, Q. & Lu, W. Mechanical and electrical properties of laminated composites containing continuous carbon nanotube film interleaves. *Compos. Sci. Tech* **127**, 113–118 (2016).
33. Yu, J. *et al*. Omnidirectionally stretchable high-performance supercapacitor based on isotropic buckled carbon nanotube films. *ACS nano* **10**, 5204–5211 (2016).
34. Xu, P. *et al*. Laminated ultrathin chemical vapor deposition graphene films based stretchable and transparent high-rate supercapacitor. *ACS nano* **8**, 9437–9445 (2014).
35. Zhao, D.-L., Li, X. & Shen, Z.-M. Electromagnetic and microwave absorbing properties of multi-walled carbon nanotubes filled with Ag nanowires. *Mater. Sci. Eng. B* **150**, 105–110 (2008).
36. Zheng, Z., Xu, B., Huang, L., He, L. & Ni, X. Novel composite of Co/carbon nanotubes: Synthesis, magnetism and microwave absorption properties. *Solid State Sci* **10**, 316–320 (2008).
37. Che, R. C., Zhi, C. Y., Liang, C. Y. & Zhou, X. G. Fabrication and microwave absorption of carbon nanotubes/$CoFe_2O_4$ spinel nanocomposite. *Appl. Phys. Lett.* **88**, 033105 (2006).
38. Feng, X. *et al*. Electrical conductivity and microwave absorbing properties of nickel-coated multiwalled carbon nanotubes/poly(phthalazinone ether sulfone ketone)s composites. *Polym. Eng. Sci.* **48**, 1007–1014 (2008).
39. Liu, G. *et al*. Enhanced electromagnetic absorption properties of carbon nanotubes and zinc oxide whisker microwave absorber. *J. Alloys Compd.* **514**, 183–188 (2012).
40. Zhao, T. *et al*. Electromagnetic wave absorbing properties of amorphous carbon nanotubes. *Sci. Rep* **4**, 5619 (2014).
41. Wang, T. *et al*. Graphene–Fe_3O_4 nanohybrids: Synthesis and excellent electromagnetic absorption properties. *J. Appl. Phys.* **113**, 024314 (2013).
42. Liu, P., Huang, Y. & Zhang, X. Superparamagnetic Fe_3O_4 nanoparticles on graphene–polyaniline: Synthesis, characterization and their excellent electromagnetic absorption properties. *J. Alloys Compd.* **596**, 25–31 (2014).
43. Chen, T. *et al*. Enhanced electromagnetic wave absorption properties of polyaniline-coated Fe_3O_4/reduced graphene oxide nanocomposites. *J. Mater. Sci.: Mater. Electron* **25**, 3664–3673 (2014).
44. Zhang, H. *et al*. Novel rGO/α-Fe_2O_3 composite hydrogel: synthesis, characterization and high performance of electromagnetic wave absorption. *J. Mater. Chem. A* **1**, 8547 (2013).
45. Liu, P., Huang, Y., Wang, L., Zong, M. & Zhang, W. Hydrothermal synthesis of reduced graphene oxide–Co_3O_4 composites and the excellent microwave electromagnetic properties. *Mater. Lett.* **107**, 166–169 (2013).
46. Ding, Y. *et al*. Reduced graphene oxide functionalized with cobalt ferrite nanocomposites for enhanced efficient and lightweight electromagnetic wave absorption. *Sci. Rep* **6**, 32381 (2016).

Author Contributions

T.W.C. and J.L. designed the experiments and wrote the paper. J.L. performed the experiments. W.L. fabricated the CNT film. J.S. fabricated the large-scale graphene. H.C. and J.Q.X. performed permittivity and permeability measurements.

Additional Information

Supplementary information accompanies this paper at doi:10.1038/s41598-017-02639-7

Competing Interests: The authors declare that they have no competing interests.

Publisher's note: Springer Nature remains neutral with regard to jurisdictional claims in published maps and institutional affiliations.